Foldable structures and the natural design of pollen grains

Eleni Katifori[a,b,1], Silas Alben[c,d], Enrique Cerda[e], David R. Nelson[a,c], and Jacques Dumais[f]

[a]Department of Physics, Harvard University, Cambridge, MA 02138; [b]Center for Studies in Physics and Biology, Rockefeller University, New York, NY 10065; [c]School of Engineering and Applied Sciences, Harvard University, Cambridge, MA 02138; [d]School of Mathematics, Georgia Institute of Technology, Atlanta, GA 30332; [e]Departamento de Física, Universidad de Santiago de Chile, Santiago, Chile; and [f]Department of Organismic and Evolutionary Biology, Harvard University, Cambridge, MA 02138

Edited by José N. Onuchic, University of California San Diego, La Jolla, CA, and approved February 25, 2010 (received for review September 29, 2009)

Upon release from the anther, pollen grains of angiosperm flowers are exposed to a dry environment and dehydrate. To survive this process, pollen grains possess a variety of physiological and structural adaptations. Perhaps the most striking of these adaptations is the ability of the pollen wall to fold onto itself to prevent further desiccation. Roger P. Wodehouse coined the term harmomegathy for this folding process in recognition of the critical role it plays in the survival of the pollen grain. There is still, however, no quantitative theory that explains how the structure of the pollen wall contributes to harmomegathy. Here we demonstrate that simple geometrical and mechanical principles explain how wall structure guides pollen grains toward distinct folding pathways. We found that the presence of axially elongated apertures of high compliance is critical for achieving a predictable and reversible folding pattern. Moreover, the intricate sculpturing of the wall assists pollen closure by preventing mirror buckling of the surface. These results constitute quantitative structure-function relationships for pollen harmomegathy and provide a framework to elucidate the functional significance of the very diverse pollen morphologies observed in angiosperms.

harmomegathy | inextensional deformation | thin shell theory | elasticity

Harmomegathy (1) is the characteristic folding of pollen grains to accommodate the decrease in cellular volume due to water loss. The partial desiccation of the pollen grain following its release from the anther results in the grain falling into a dormant state that ensures the cellular material survives until the pollen grain reaches the stigma of a flower. Upon capture by the stigma, the pollen grain is once again exposed to a humid environment, resumes its hydrated condition, and harmomegathy is reversed (2, 3). The apertures on the pollen surface provide the main routes for exchange with the environment (3) and serve as exit points for the pollen tube. The structure of the pollen wall is designed to allow the apertures to fold inwardly during harmomegathy thus reducing the rate of water loss. Therefore, harmomegathy can be interpreted as an elegant solution to two conflicting demands on the pollen grain—the requirement to maintain routes of exchange between the grain and the environment and the need to limit the desiccation of the cellular material (Fig. 1*A*).

The pollen wall has a complex composite structure (Fig. 1*B*). The outer layer known as exine is rich in sporopollenin—a stiff, chemically resistant, and water impermeable biomaterial. The cellulosic intine forms a compliant, water permeable layer that lies just inside the exine and is firmly attached to it. The intine is only exposed at the apertures where the exine is interrupted (Fig. 1*B*). The number, arrangement, and shape of the apertures greatly influence the pollen grain folding pathway (4–7). During dehydration, aperturate pollen grains become increasingly elongated, with the aperture margins approaching each other so that the pollen grain becomes effectively sealed (Fig. 1 *C* and *D*). The compliant apertures provide preferred sites of invagination that guide the folding. On the other hand, pollen grains that lack elongated apertures respond to desiccation by forming depressions on the exine whose number and location can vary greatly (Fig. 1 *E* and *F*). The importance of wall structure in guiding harmomegathy was recognized as early as 1883 (8), and although more recent work has reinforced this idea (5, 9, 10), there is still no theory to support the many claims about the function of the pollen wall as a harmomegathic apparatus. Here, we provide a first detailed quantitative analysis of the structure-function relationship for pollen harmomegathy.

Results and Discussion

To understand how the different folding pathways emerge, we must consider the mechanical response of a closed shell to a reduction of its volume. Exact solutions for large deformation of a shell are difficult to obtain. However, it is possible to derive approximate solutions to the problem based on geometric considerations only. Central to our approach is the classic result for thin-walled shells that bending deformations (i.e. changes in the surface curvature) are energetically more favorable than stretching deformations (11). Thus, closed-form approximate solutions for large deformation of thin shells can be found by considering inextensional (bending-only) deformations of the initial geometry.

Pogorelov (11) showed that for a closed convex surface such as a sphere the only possible inextensional deformation is a mirror reflection of a segment of the surface about a dissecting plane. This solution provides a good approximation of the folding pathway observed in porate and inaperturate pollen grains (Fig. 1 *E* and *F*). By virtue of being a bending-only deformation of the original surface, one can surmise that mirror buckling is a minimal energy solution for pollen folding when large apertures are absent as demonstrated for nonbiological systems (12). In closed shells with finite wall thickness, pure bending is not possible without some stretching. Since stretching is energetically costly, it is concentrated along ridges and cusps (11–13) as those observed in the pollen grains of *Aristolochia* and corn (Fig. 1 *E* and *F*).

Applying these considerations to aperturate pollen grains, we would expect the harmomegathic wall deformation to be primarily accommodated by bending of the thin but stiff exine, with most of the stretching being concentrated at the apertural site where the exine is reduced or completely absent. To test this prediction, we used environmental scanning electron microscopy to observe the folding pathway in lily (*Lilium longiflorum*) and *Euphorbia milii* pollen (Fig. 2 *A* and *D* (see Movies S1 and S2 for the folding process). The apertural and interapertural regions differ

Author contributions: E.K., S.A., E.C., D.R.N., and J.D. designed research; E.K., S.A., E.C., and J.D. performed research; E.K., E.C., D.R.N., and J.D. contributed new reagents/analytic tools; E.K., S.A., E.C., and J.D. analyzed data; and E.K., D.R.N., and J.D. wrote the paper.

The authors declare no conflict of interest.

This article is a PNAS Direct Submission.

[1]To whom correspondence should be addressed. E-mail: ekatifori@mail.rockefeller.edu.

This article contains supporting information online at www.pnas.org/cgi/content/full/0911223107/DCSupplemental.

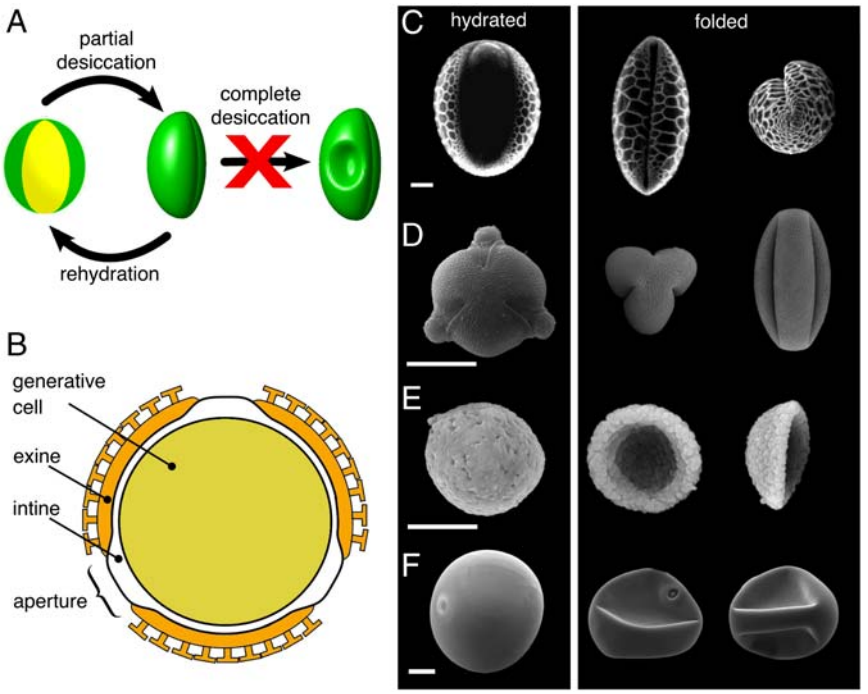

Fig. 1. Harmomegathy in pollen grains. (*A*) Folding of aperturate pollen grains in response to change in humidity allows a partial dehydration of the cellular material while preventing complete desiccation and death. (*B*) Wall structure of a typical tricolpate (tri- aperturate) pollen grain. (*C*)—(*F*) SEM images of pollen grains in their unfolded (hydrated) and folded states. (*C*) The monosulcate pollen grain of *Lilium longiflorum*. In the hydrated state, the intine is visible at the aperture, where the exine is absent. In the folded state, the aperture has invaginated. (*D*) The tricolpate pollen grain of *Euphorbia milii*. The aperture protrudes in the hydrated state but retracts completely within the pollen in the folded state. (*E*) The inaperturate pollen of *Aristolochia gigantea*. Harmomegathy is reduced to a mirror buckling of the pollen wall. (*F*) The monoporate pollen grain of maize (*Zea mays*). Scale bar, 20 μm.

strikingly in their behavior. The apertural wall crumbles into sharp folds before disappearing inside the grain while the interapertural region rolls gradually into a spindle shape.

We ask whether this type of pollen folding can be reduced to a bending deformation of the stiff exine interrupted at the apertural sites. The requirement that the surface should not stretch has one important geometrical implication—the Gaussian curvature K of the surface must be preserved during folding (14). For an axisymmetric surface, the Gaussian curvature takes a simple form if the surface is parameterized using the meridional arclength, s, and the radial distance, $r(s)$, from the axis of rotation (Fig. 2 *G* and *H*). The Gaussian curvature is then

$$K(s) = -r''(s)/r(s), \qquad [1]$$

where the double prime denotes the second derivative with respect to s (see *Appendix*). If $r_0(s)$ defines an axisymmetric surface with Gaussian curvature $K(s)$ then, according to the relation above, the family of surfaces $r(s,t) = \alpha(t)r_0(s)$ will also have the same Gaussian curvature. Here $\alpha(t)$ is an arclength independent parameter that allows a continuous inextensional transition between the different surfaces.

We used this approach to predict pollen folding taking the outline of the hydrated grain as initial geometry [i.e. $r(s,0) = r_0(s)$]. For the lily pollen, decreasing gradually the parameter α from its initial value $\alpha(0) = 1$ leads to the characteristic cigar shape observed during harmomegathy (Fig. 2 *B* and *G*). For the triaperturate pollen of euphorbia, the surface is subdivided into three identical interapertural elements with $r_0(s)$ now representing the equatorial outline of the hydrated pollen (Fig. 2*H*). Increasing the parameter α above one leads to folding of these elements and closure of the pollen grain (Fig. 2 *E* and *H*). The match between the closed-form solutions and the observed folding is surprisingly accurate verifying that the dominant mode of folding is consistent with an inextensional bending of the pollen wall.

A useful approach to check that the folding of pollen grains adheres to an inextensional deformation is based on the scaling of the pollen outline, as can be obtained from environmental scanning electron micrographs. Given the form $r(s,t) = \alpha(t)r_0(s)$ for the inextensional deformation of a surface of revolution, normalizing the pollen outlines by the equatorial radius $r(0,t)$ gives $r(s,t)/r(0,t) = r_0(s)/r_0(0)$. Therefore, it is possible to collapse all the pollen outlines onto the same master curve. Applying this normalization to the lily pollen shows that the outlines follow the same master curve (Fig. 3). The constant length of these meridional outlines verifies the inextensibility of the meridians and implies, through the collapse of the curves when normalizing by $r(0,t)$, an angular displacement compatible with the sealing of the aperture and inextensibility of the parallels.

The closed-form inextensional solutions lead to point and line defects where one of the two principal curvatures of the surface is infinite (e.g. the poles in Fig. 2*B*). In a shell with nonzero wall thickness, these defects would be associated with infinite bending energies. We can therefore expect pollen grains to develop stretching at these locations to avoid infinite curvatures and infinite energies. To incorporate these aspects of the folding pathway, we performed numerical simulations with a tethered mesh discretization (15) of the pollen wall. The bending and stretching energies of the tessellated pollen were calculated using a mass-spring model (see *Materials and Methods* and *SI Text*). The results of the numerical simulations for lily and euphorbia show that in both cases the pollen grain elongates and the aperture margins roll in to seal the furrow (Fig. 2 *C* and *F*). The close match between the simulations and the observed pollen geometry establishes that pollen wall structure is the main determinant of the folding pathway. The simulations also permit quantitative predictions regarding the bending and stretching energy density

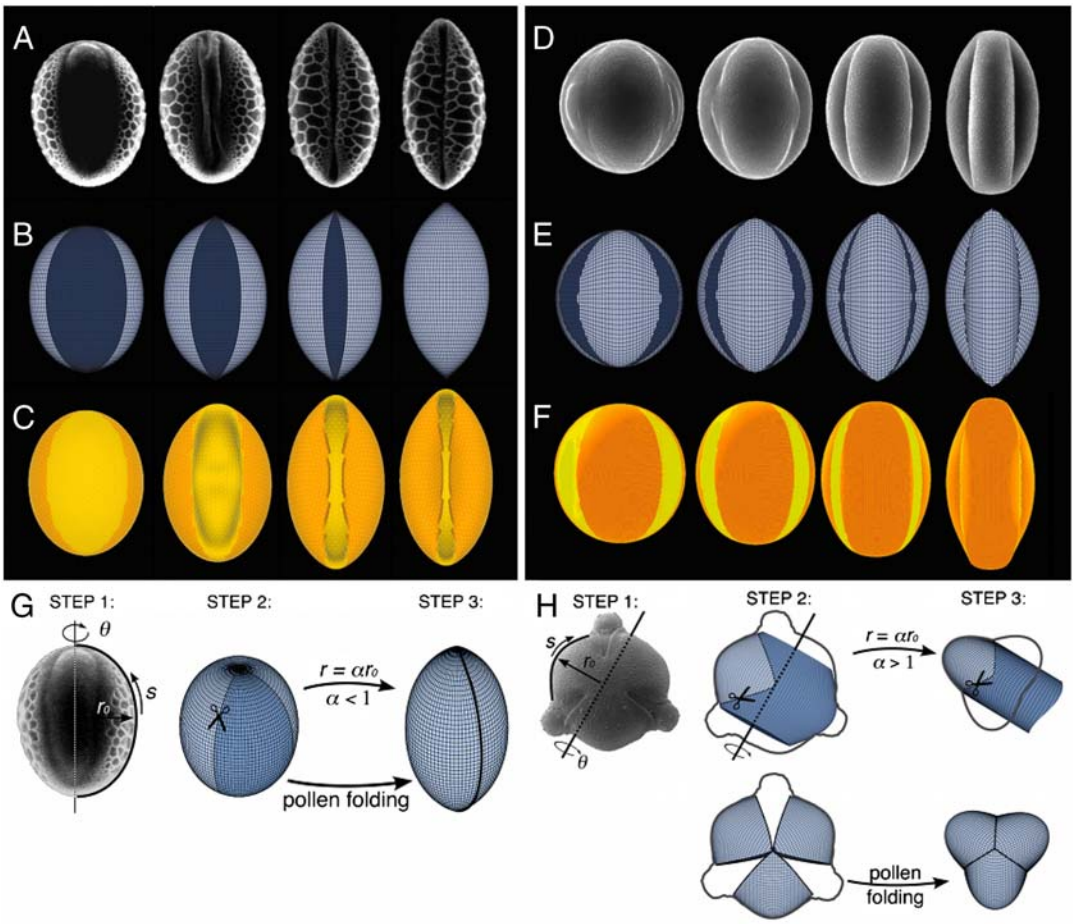

Fig. 2. Folding pathways for monosulcate pollen (*Lilium longiflorum, left*) and tricolpate pollen (*Euphorbia milii, right*). (*A*) and (*D*) Sequential scanning electron micrographs of desiccating lily and euphorbia pollen grains. (*B*) and (*E*) Inextensional solutions for the exine folding. (*C*) and (*F*) Numerical simulations of the folding. (*G*) The "monosulcate fold" as observed in lily pollen. Step 1: rotate the meridional outline of the hydrated pollen grain around the pollen axis to create a surface of revolution. Step 2: remove the segment corresponding to the aperture. Step 3: fold the surface using the relation $r = \alpha r_0$ with $\alpha < 1$. (*H*) The tricolpate fold as observed in euphorbia pollen. Step 1: rotate the equatorial outline of one of the three interapertural regions around the axis to create a surface of revolution. Step 2: excise three segments corresponding to the interapertural exine (light regions) to assemble a complete hydrated pollen grain. Step 3: fold the surface using the relation $r = \alpha r_0$ with $\alpha > 1$ and excise the three segments corresponding to the interapertural exine to assemble a complete folded pollen grain.

profile of the wall of a folded pollen grain. The stretching energy density profile is dominated by the high stretching regions at the locations associated with the singularity of the zero thickness solution (see Fig. 4). Deviation from the geometrical (zero wall thickness) model results in condensation of stretching in the neighborhood of those locations. Similarly, deviation from the axisymmetry of the geometrical model results in bending energy density patterns that are not uniform around the circumference.

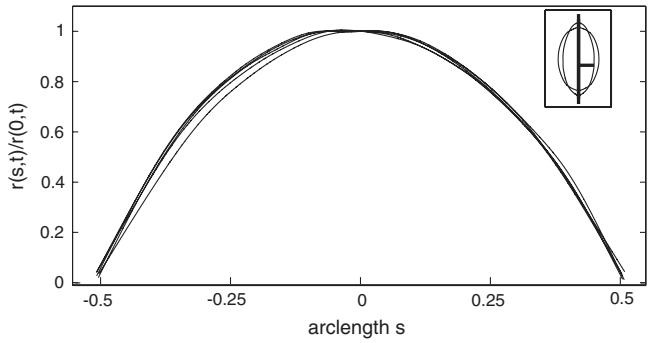

Fig. 3. Normalization of the lily pollen grain meridional outlines by the equatorial radius. All curves collapse onto one master curve. Inset, pollen grain meridional outlines (hydrated and fully folded) in Cartesian coordinates. The outlines were obtained from environmental scanning electron micrographs.

To determine how aperture geometry contributes to harmomegathy, we performed a series of simulations varying the apertural design while keeping the initial pollen shape and wall material properties constant (Fig. 5). Elongated apertures that almost reach the poles of the pollen grain (Fig. 5*A*) or that span half the equator (Fig. 5*C*) allow for successful closure. This result is consistent with the inextensional solution which requires that a segment spanning the two poles be removed to allow folding. The bending and stretching energy densities of the folded shape indicate that the pollen grain undergoes harmomegathy with very little stretching. If the aperture is shorter, the pollen is prevented from adequately sealing the aperture, and a considerable amount of stretching appears at the aperture margin (Fig. 5*B*). If the volume is decreased further, the pollen grain ultimately assumes the mirror-buckling geometry as in Fig. 5*E*. Finally, porate pollen grains adopt quickly the mirror-buckling geometry with a considerable amount of stretching energy concentrated at the rim (Fig. 5*D* and *SI Text*). We thus see that in the framework of a simple two-material thin shell mechanical model, the shell geometry couples with the shape of the aperture to produce significantly different folded shapes. We conclude that pollen grains

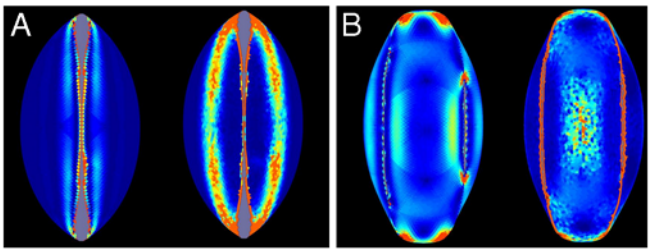

Fig. 4. Stretching and bending energies in folded pollen grains. (*A*) Computed bending (left) and stretching (right) energy densities in the lily pollen grain. (*B*) Computed bending (left) and stretching (right) energy densities in the euphorbia pollen grain. Red indicates high energy density (note: the energy scales are in arbitrary units but are kept constant in (*A*) and (*B*).

have evolved long apertures to guide folding away from mirror-buckling and toward self-sealing solutions.

Further evidence that the exine has evolved to favor the self-sealing folding pathway over other modes of deformation is seen in the exine sculpturing of lily pollen (Fig. 6) and numerous other species (9). Volume accommodation via mirror buckling requires that part of the exine becomes concave thus forcing the pilea of the outer exine against each other (Fig. 6*B*). On the other hand, volume accommodation in aperturate pollen leaves the surface convex except over the aperture where the exine is absent. The pilea thus remain separated and are mechanically inactive. Given that the bending stiffness of the wall scales as the cube of the wall thickness (11), even a modest increase in the effective thickness due to pilea interaction can have a great impact on the total bending energy of the shell. Therefore, the system of pilea that decorate the exine is an ingenious way to modulate the effective wall thickness; making mirror buckling an unfavorable mode of deformation.

The structural design of pollen grains can thus be interpreted as guiding harmomegathy along competing folding pathways. Under most circumstances, mirror buckling allows thin spherical shells to accommodate volume change with minimal stored elastic energy (11, 12). Pollen grains with inaperturate, homogeneous exines naturally follow this folding pathway (Fig. 1 *E* and *F*) as well as those equipped with short apertures (Fig. 5 *D* and *E*). The

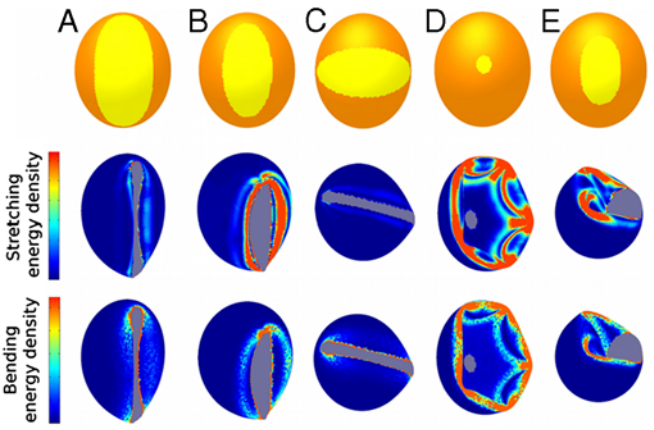

Fig. 5. Energetics of pollen wall deformation for different apertural shapes. The initial geometry of the pollen grain (ellipsoid of revolution, ratio of long R_L to short R axis equal to $R_L/R = 1.2$), ratio of bending moduli of intine κ_I, and exine κ_E equal to $\kappa_I/\kappa_E = 0.015$, thicknesses $h_E/R = 1/50$ and $h_I/R = 1/25$ are the same for (*A*)–(*E*). The top row represents the turgid geometry, the lighter color indicating the position of the aperture. The middle and bottom rows indicate the stretching and bending energy density of the exine, respectively (orange color: high energy; blue color: low energy). The color scheme for the stretching and bending energy density is in arbitrary units but was kept constant for all the cases shown.

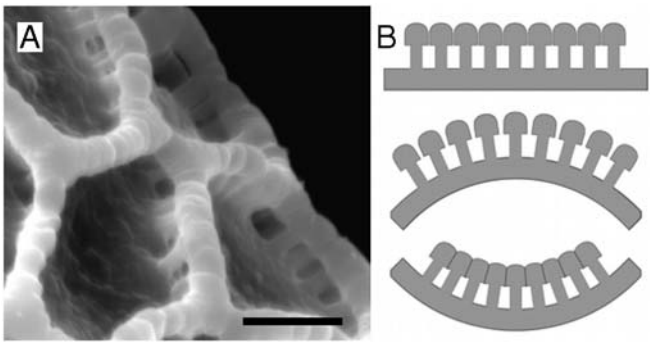

Fig. 6. The network of pilea of the outer exine (ectexine) supports the pollen wall and prevents mirror buckling. (*A*) SEM micrograph of the lily pollen exine showing rows of pilea buttressing the wall (scale bar, 5 μm). (*B*) Schematic representation of the mechanical asymmetry of the buttressed exine. For deformations that make the surface convex, the pilea move apart (middle panel) and are therefore mechanically inactive. For a concave deformation of the exine surface, the pilea are forced against each other (*bottom*) thus increasing the bending stiffness of the wall.

folding transition is mediated by a narrow, high energy ridge connecting two regions of opposite curvature. Some intriguing biological systems such as the Venus flytrap (16) deform in a similar manner and have inspired the design of artificial responsive surfaces (17, 18). Although mirror buckling is a common deformation pathway, it requires transition through a high energy state often leading to bistability. This design problem is elegantly solved by the folding pathway observed in aperturate pollen. Here, the exine deforms along a continuous path of inextensional shapes without the need for a ridge of high stretching energy. This property softens the transition and allows responsiveness of the pollen wall to slight humidity changes in the environment. The graded response opens up a suite of technological applications that cannot be achieved with bistable transitions. The design principles uncovered in pollen as well as the vast number of pollen grain morphologies (19) can serve as a source of tested solutions for the development of smart surfaces that can respond and adapt to their environment.

Materials and Methods

Plant Material and Microscopy. Fresh pollen collected from flowers of *Lilium longiflorum*, *Euphorbia milii*, *Aristolochia gigantea*, and *Zea mays* was used directly or kept frozen until needed. For microscopic observations, hydrated pollen grains were fixed in 2,2 dimethoxypropane (7), critical point dried, sputter coated with gold, and imaged in an FEI Quanta scanning electron microscope (SEM). Dried pollen grains were sputter coated and imaged without prior fixation. To visualize the folding process, fresh pollen was used directly in the environmental mode of the microscope. The outlines presented in Fig. 3 were obtained from such environmental SE micrographs. The error in the determination of the outlines is of the order of the thickness of the lines. The major source of experimental error comes from the inability to precisely control the pollen grain orientation with respect to the optical axis.

We determined the wall geometrical parameters of lily pollen grains from freeze-fractured material observed under the SEM. The combined thickness of the intine and exine away from the sulcus is 1.5–2.0 μm whereas the thickened apertural intine measures 3–4 μm, values that agree well with the literature (20). The lily pollen grain geometry is closely fitted by a prolate spheroid with a minor axis of 90 μm and major axis of 110 μm. For the euphorbia pollen, we used electron microscopy to determine the hydrated geometry and aperture shape of the pollen grain. We found that the shape of the hydrated pollen grain is well fitted by a slightly deformed sphere $R(\phi, \theta) = 15\ \mu\text{m}(1 - 0.02|\cos(\theta)|\sin 3\phi)$ where ϕ is the azimuthal angle and θ the latitudinal angle. The exine thickness (1.1–1.7 μm) and apertural intine thickness (1.4 μm) were determined with light microscopy.

Simulation of Pollen Folding. To model harmomegathy for a pollen wall of finite thickness, we used a tethered mesh discretization of the pollen surface, initially developed in the context of polymeric surfaces (15). In the tethered mesh, all bonds have approximately the same length and each grid point has

six nearest neighbors, except for the inevitable 12 points for spherical topologies which have only five neighbors. To test whether the fivefold "defects" of the tessellated mesh have an effect on the folding pathway, we performed simulations changing their position on the model pollen grain and found that there was little variation in the results, the most important difference being a slight asymmetry of the in-rolled margins of the aperture.

In our simulation, all key geometrical parameters were measured directly (see above). However, the Young's modulus of sporopollenin and the cellulosic intine are not known except for one measurement for the exine of ragweed pollen (21). We set the Poisson ratio to $\nu = 1/3$, leaving us with one free parameter in the model, the ratio of the Youngs modulus of the intine E_I and exine E_E. The simulations presented in this work were performed at a small intine to exine bending modulus ratio $\kappa_I/\kappa_E < 0.015$. To determine how sensitive the pollen grain folding is to the value of the Youngs modulus, we performed numerical simulations for an ellipsoidal pollen grain for various modulus ratios and compared the optimum sealing states, defined as the folded geometry that minimizes the distance of the apertural margins at the equator. We found that the folded shape is robust over a wide range of modulus ratios (see *SI Text*).

The bending (H_b) and stretching (H_s) energies of the tessellated pollen were calculated using a mass-spring model with the spring rest lengths and angles chosen so that the initial pollen geometry is stress free. This choice was dictated by our observations that isolated wall fragments retain the geometry of the hydrated condition, despite the absence of cellular material (22). The discretized stretching energy of the pollen grain, modeled as a thin elastic shell is

$$H_s = \frac{1}{2}\sum_{<ij>} \epsilon_{ij}(|\vec{r}_i - \vec{r}_j| - \rho_{ij})^2, \qquad [2]$$

where $\vec{r}_i$ is the position of the nodes of the mesh, ρ_{ij} is the equilibrium length of the bond joining nodes i and j, and the summation $\langle ij \rangle$ is over adjacent vertices (15, 23). The equilibrium lengths were chosen to relax the strains associated with the 5-fold coordinated points and suppress spurious buckling transitions (24). Depending on whether the bond of the pair ij is assigned to the aperture or interapertural region of the wall, the discretized stretching modulus takes the values ϵ_I and ϵ_E, respectively.

The discretized bending energy is

$$H_b = -\frac{1}{2}\sum_{<kl>} \kappa_{kl}\cos(\theta_{kl} - \theta^0_{kl})^2, \qquad [3]$$

where θ_{kl} is the angle between the normals of adjacent triangular faces k and l of the tessellated surface, whereas θ^0_{kl} is the equilibrium angle determined by the spontaneous curvature, that is the shell curvature at the initial stress free state. The parameter κ_{kl} is proportional to the bending rigidity of the surface and, similar to the stretching modulus, takes the value κ_E at the exine and κ_I at the aperture.

To enforce self-avoidance of the shell during the deformation, the nodes of the shell were assigned a "hard core" repulsive potential with range equal to one third of the average tether length. To impose the fixed volume constraint, we added a quadratic term of the form

$$H_V = \lambda(V - V_0)^2, \qquad [4]$$

where V is the volume of the pollen and V_0 is a target volume (25).

Pollen dehydration proceeds over a period of 1 min or more. Inertial effects are thus unimportant and the folding is dominated by energetics. The equilibrium volume of the pollen grain depends on the atmospheric humidity (26), which provides a fixed volume constraint. The shape of the folding pollen grains should be determined by minimizing the total elastic energy $H_s + H_b$ for the fixed volume. The shell shape that minimized the sum of the elastic energy and the volume constraint term was found using either an adaptive step gradient descent or conjugate gradient scheme. The parameter λ was initially chosen sufficiently small to allow convergence and gradually increased until $(V - V_0)/V < 10^{-5}$ (25).

Appendix

The Gaussian curvature of a doubly curved surface is the product of the two principal curvatures, c_s and c_θ, where s and θ are the meridional and azimuthal coordinates. The meridional curvature is $c_s = -r''/(1 - r'^2)^{1/2}$ and the circumferential curvature is $c_\theta = (1 - r'^2)^{1/2}/r$ where r is the distance from the axis of rotation and the prime and double prime denote the first and second derivatives with respect to the arclength s. The Gaussian curvature of the surface is thus $K(s) = c_s c_\theta = -r''(s)/r(s)$. During folding, the Gaussian curvature must be preserved. This property can be used to predict families of surfaces that are isometric. According to the definition above, the family of surfaces $r(s,t) = \alpha(t) r_0(s)$ all share the same Gaussian curvature $-r_0''(s)/r_0(s)$. Here α is a parameter greater than zero that allows a gradual transition between the different surfaces. When the angular displacement changes inversely with α allowing the closure of the pollen grain, the parameter α does not appear in the first fundamental form (14). Thus, this family of curves represents a pure bending transformation.

ACKNOWLEDGMENTS. We thank the Center for Nanoscale Systems (Harvard) for use of their microscope facility. E.C. acknowledges financial support from Fondecyt (Grant 7050276). Work by E.K. and D.R.N. was supported in part by the National Science Foundation through Grant DMR-0654191 and through the Harvard Materials Research Science and Engineering Center via Grant DMR-0820484.

1. Wodehouse RP (1935) *Pollen Grains* (McGraw-Hill, New York).
2. Heslop-Harrison J (1979) An interpretation of the hydrodynamics of pollen. *Am J Bot* 66:737–743.
3. Heslop-Harrison J (1979) Pollen walls as adaptive systems. *Ann Mo Bot Gard* 66:813–829.
4. Thanikaimoni G (1986) Pollen apertures: Form and function. *Pollen and Spores: Form and Function*, eds S Blackmore and IK Ferguson (Academic, London), pp 119–136.
5. Payne WW (1972) Observations of harmomegathy in pollen of anthophyta. *Grana* 12:93–98.
6. Blackmore S, Barnes SH (1986) Harmomegathic mechanisms in pollen grains. *Pollen and Spores: Form and Function*, eds S Blackmore and IK Ferguson (Academic, London) p 137.
7. Heidemarie Halbritter, Michael Hesse (2004) Principal modes of infoldings in tricolp(or) ate angiosperm pollen. *Grana* 43:1–14.
8. Vesque J (1883) Sur l'organization mecanique du grain de pollen. *Comptes Rendus de l'Académie des Sciences* 96:1684–1686.
9. Bolick MR (1981) Mechanics as an aid to interpreting pollen structure and function. *Rev Palaeobot Palyno* 35:61–79.
10. Muller J (1979) Form and function in angiosperm pollen. *Ann Mo Bot Gard* 66:593–632.
11. Pogorelov Aleksei Vasilevich (1988) *Bendings of Surfaces and Stability of Shells* (AMS Bookstore, Providence, RI).
12. Quilliet C, Zoldesi C, Riera C, van Blaaderen A, Imhof A (2008) Anisotropic colloids through non-trivial buckling. *Eur Phys J E* 27:13–20.
13. Witten TA (2007) Stress focusing in elastic sheets. *Rev Mod Phys* 79:643–675.
14. Struik Dirk J (1957) *Lectures on classical differential geometry* (Addison-Wesley, Reading, MA).
15. Kantor Yacov, Nelson David R (1987) Phase transitions in flexible polymeric surfaces. *Phys Rev A* 36:4020–4032.
16. Forterre Y, Skotheim JM, Dumais J, Mahadevan L (2005) How the venus flytrap snaps. *Nature* 433:421–425.
17. Holmes DP, Crosby AJ (2007) Snapping surfaces. *Adv Mat* 19:3589–3593.
18. Sugiyama Y, Hirai S (2006) Crawling and jumping by a deformable robot. *Int J Robot Res* 25:603–620.
19. Kesseler R, Harley M (2004) *Pollen: The Hidden Sexuality of Flowers* (Papadakis Publisher, London).
20. Sumio Nakamura (1979) Development of the pollen grain wall in *Lilium longiflorum*. *J Electron Microsc* 28:275–284.
21. Liu T, Zhang Z (2004) Mechanical properties of desiccated ragweed pollen grains determined by micromanipulation and theoretical modelling. *Biotechnol Bioeng* 85:770–775.
22. Rowley J, Skvarla J (2000) The elasticity of the exine. *Grana* 39:1–7.
23. Seung HS, Nelson David R (1988) Defects in flexible membranes with crystalline order. *Phys Rev A* 38:1005–1018.
24. Jack Lidmar, Leonid Mirny, Nelson David R (2003) Virus shapes and buckling transitions in spherical shells. *Phys Rev E* 68:051910.
25. Antonio Šiber (2006) Buckling transition in icosahedral shells subjected to volume conservation constraint and pressure: Relations to virus maturation. *Phys Rev E* 73:061915.
26. Aylor Donald E (2003) Rate of dehydration of corn (Zea mays L.) pollen in the air. *J Exp Bot* 54:2307–2312.